Journal of Materials Chemistry A

PAPER

View Article Online
View Journal

Cite this: DOI: 10.1039/c6ta06442f

Structure–reactivity relationship in Co_3O_4 promoted Au/CeO_2 catalysts for the CH_3OH oxidation reaction revealed by *in situ* FTIR and *operando* EXAFS studies†

M. Manzoli,*[a] F. Vindigni,[b] T. Tabakova,[c] C. Lamberti,[bf] D. Dimitrov,[d] K. Ivanov[d] and G. Agostini[eg]

Received 28th July 2016
Accepted 20th December 2016

DOI: 10.1039/c6ta06442f

www.rsc.org/MaterialsA

A strong influence of the amount of the Co_3O_4 promoter on the catalytic performance in methanol oxidation of different gold catalysts supported on ceria was observed. The activity followed the order: Au/10 wt% Co_3O_4-doped CeO_2 > Au/5 wt% Co_3O_4-doped CeO_2 > Au/15 wt% Co_3O_4-doped CeO_2 > Au/CeO_2 ≫ Au/Co_3O_4. FTIR measurements of adsorbed CO indicate that oxidized gold sites are initially present on the activated samples and that such species are involved in the methanol reaction. Methanol oxidation performed under static conditions gave rise at 75 °C to mainly formate species on Au/CeO_2 and to a large variety of different carbonate species on Au/10 wt% Co_3O_4-doped CeO_2. FTIR and EXAFS analyses revealed that the active sites present on the best performing Au/CeO_2 catalyst added with 10 wt% Co_3O_4 are oxidized gold species, close to Co sites, at the interface with the support, which are reduced under reaction conditions. These species are able to activate and to react with oxygen giving rise to formate and carbonate species.

Introduction

Supported gold nanoparticles attract significant attention due to their high catalytic activity in various oxidation reactions at low temperatures. The catalytic oxidation of Volatile Organic Compounds (VOCs), such as methanol, is a subject of considerable interest due to their relevance in many industrial applications as well as in the field of sustainable chemistry. These catalytic processes have been considered as some of the most efficient ways to reduce harmful emissions from various chemical industries. Over the past two decades gold-based catalysts have been proven to be effective for many reactions of environmental significance.[1]

Considerable emphasis is placed on the catalyst preparation and on the selection of the support.[2] The oxidation activity of gold catalysts is closely related to the size of the Au particles[3] and to the ability of the support to provide active oxygen species. For this reason, selection of an appropriate support is a critical factor.

Ceria is very attractive, due to its ability to maintain high metal dispersion and to change Ce oxidation state depending on the redox conditions. The rapid change of oxidation state is related to its ability to store and release oxygen, a property measured by the "oxygen storage capacity" (OSC),[4] which results in rapid formation and elimination of oxygen vacancy defects.[5] These characteristics make CeO_2 a very interesting support for oxidation reactions.

In principle, the modification of ceria can increase the concentration of oxygen vacancies and a strong influence of the nature of the added oxide (Me = Fe, Mn, Sn) on the catalytic performances was observed recently by some of us.[6] For example, it was reported that the modification of CeO_2 with different Zr amounts leads to increased catalytic activity in the CO oxidation,[7] as well as in the Water Gas Shift reaction[8] and in the steam reforming of methanol.[9] Moreover, gold catalysts supported on iron-modified ceria oxides containing appropriate molar percentages of Fe were proved to be more active than unmodified Au/CeO_2 for total and preferential CO oxidation[10,11] and for the Water Gas Shift reaction.[12]

The beneficial influence of cobalt oxide on the CO oxidation behaviour of Au/CoO_x/CeO_2–Al_2O_3 systems was previously

[a]Department of Drug Science and Technology, NIS Interdepartmental Centre, University of Torino, Via P. Giuria 9, 10125 Torino, Italy. E-mail: maela.manzoli@unito.it

[b]Department of Chemistry, NIS Interdepartmental Centre, University of Torino, Via P. Giuria 7, 10125 Torino, Italy

[c]Institute of Catalysis, Bulgarian Academy of Sciences, 1113 Sofia, Bulgaria

[d]Department of Chemistry, Agricultural University, 4000 Plovdiv, Bulgaria

[e]Leibniz Institute for Catalysis at the University of Rostock (LIKAT), Albert-Einstein-Str. 29A, D-18059 Rostock, Germany

[f]IRC "Smart Materials", Southern Federal University, Zorge Street 5, 344090 Rostov-on-Don, Russia

[g]European Synchrotron Radiation Facility, 38043 Grenoble, France

† Electronic supplementary information (ESI) available: Fig. S1–S6. See DOI: 10.1039/c6ta06442f

shown.[13] It was found that the catalytic activity depends on the cobalt loading, which provides a submonolayer coverage of the support surface, where a CoO_x–CeO_2 interaction takes place giving rise to a synergism between Co and Ce redox properties. Indeed, Co_3O_4 itself was demonstrated to be very active in the sub-ambient CO oxidation reaction depending on the morphology and on the preferential exposition of the [1 1 0] plane in which the highest number of Co(III) sites are present.[14,15]

Three dimensionally ordered macroporous Au/CeO_2–Co_3O_4 catalysts showed enhanced CO preferential oxidation in H_2-rich gas mixtures[16] and formaldehyde oxidation.[17] The former paper proposed that the origin of the high CO conversion and CO_2 selectivity was the presence of ionic Au in intimate contact with CeO_2. In the latter one, a mechanism involving the synergistic effect between CeO_2 and Co_3O_4 supports, which greatly accelerates the surface active oxygen migration and activates the Au species, was proposed to explain the improvement in the catalytic HCHO oxidation. It was established that Au/CeO_2–CoO_x catalysts prepared by mechano-chemical activation exhibited much higher activity in the reaction of complete benzene oxidation than that prepared using coprecipitation.[18] The reason for this different catalytic behaviour was the existence of a Co-containing phase with enhanced redox properties that influenced both gold and modified ceria in close vicinity. Therefore, ceria supports with different amounts of Co_3O_4 were prepared by mechano-chemical activation in order to optimize the content of the promoter. Recently, we observed a strong influence of the nature of the added oxide on the activity of ceria-based gold catalysts for catalytic abatement of CO in waste gases.[19] In particular, a gold catalyst supported on ceria modified by Co_3O_4 exhibited the best performance: a 100% CO conversion degree was achieved at 25 °C. The support with a composition 90 wt% CeO_2 and 10 wt% Co_3O_4 was beneficial for the nucleation and growth of highly dispersed gold. In this system, a synergy between gold and the Co-doped ceria support causes significant enhancement in the reducibility and capability for oxygen activation, which resulted in improved oxidation activity. However, a clear correlation between the catalytic activity and the nature and structure of the active sites has not been fully established yet.

The correlation existing between catalyst structure and catalytic activity/selectivity is the main goal in research applied to catalysis.[20] In principle, EXAFS/XANES can give relevant complementary information on the structural and electronic properties of such systems.[21–25] In addition, FTIR spectroscopy represents a powerful technique to investigate the surface sites at an atomic level. In particular, the analysis of FTIR spectra of adsorbed probe molecules allows us to understand the nature and the abundance of the exposed active sites as well as to have detailed information on their chemical environment.[26–30] Therefore, the use of these techniques can assist in the comprehension of the parameters ruling the unique catalytic properties of gold catalysts, as well as to implement the knowledge in the design of new systems. Keeping in mind these purposes, the aim of this work was an accurate EXAFS and FTIR study on the nature of the active sites exposed at the surface of highly dispersed gold catalysts supported on ceria modified by different amounts of Co_3O_4. Research efforts were focused to achieve information on the local structure of the active sites in terms of position of cobalt atoms with respect to the gold metallic phase.

Experimental

Materials

Cerium hydroxide was synthesized by precipitation of aqueous solutions of $Ce(NO_3)_3 \cdot 6H_2O$ with K_2CO_3 at constant pH = 9.0 and at a temperature of 60 °C, aging at the same temperature for 1 hour, filtering, washing until removal of NO_3^- ions and drying in vacuum at 80 °C. Mixed CeO_2–Co_3O_4 supports were prepared by a simple mechano-chemical mixing procedure: a mixture of cerium hydroxide and 5, 10, 15 wt% of laboratory-made Co_3O_4 was subjected to mechano-chemical milling for 30 min in a mortar and calcination at 400 °C for 2 hours. Hereafter the supports will be labelled as Ce5Co, Ce10Co and Ce15Co depending on cobalt oxide loading in wt%. Gold catalysts (3 ± 0.05 wt%) were prepared by the deposition–precipitation method at constant pH 7 and temperature 60 °C. Gold was deposited on a mixed metal oxide support preliminarily suspended in water and activated in an ultrasound disintegrator under vigorous stirring. Hereafter catalysts will be labelled as AuCe5Co, AuCe10Co and AuCe15Co depending on cobalt oxide loading in wt%.

The deposition–precipitation was carried out in an automated laboratory reactor under full control of all preparation parameters (pH, temperature, stirring speed, reactant feed flow rates, *etc.*). After aging at 60 °C within 1 h, filtering and careful washing, the precursors were dried under vacuum at 80 °C and calcined in air at 400 °C for 2 hours. Moreover, unmodified Au/CeO_2 and Au/Co_3O_4 (hereafter labeled as AuCe and Au/Co_3O_4, respectively), used as blank samples, were also prepared by the deposition–precipitation method under the conditions described above. All initial salts used were 'analytical grade'.

Catalytic activity measurements

The catalytic activity of the samples in CH_3OH oxidation was measured using an isothermal plug flow reactor within a different temperature range. The following conditions were chosen: catalyst bed volume – 0.5 g (particle size 0.6–1.0 mm), inlet CH_3OH concentrations – 2.0% balanced with air and space velocity 10 000 h^{-1}. The tests were carried out by increasing the reaction temperature stepwise until complete CH_3OH oxidation. The degree of conversion was measured at every 20 °C step after stationary conversion was achieved. The behaviour was also studied during decrease of the temperature down to room temperature, again stepwise. The conversion data at increasing and decreasing temperature match well. The duration of catalytic test for each sample was about 8 hours. The reactant and product gases were analysed for methanol, CO, CO_2, O_2 and N_2 using a HP 5890 Series II gas-chromatograph, equipped with flame ionization and thermal conductivity detectors and Porapak Q and MS-5A columns.

Methods

The amount of gold in all samples was analyzed by atomic absorption spectroscopy (Varian Vista MPX) and the values determined were 3 (±0.05) wt% Au.

High resolution transmission electron microscopy (HRTEM) measurements were performed using a side entry Jeol JEM 3010 (300 kV) microscope equipped with a LaB_6 filament and fitted with X-ray EDS analysis equipment using a Link ISIS 200 detector. For analyses, the powdered samples were deposited on a copper grid, coated with a porous carbon film. All digital micrographs were acquired using an Ultrascan 1000 camera and the images were processed with a Gatan digital micrograph. A statistically representative number of Au particles (*i.e.* 250 for each sample) were counted in order to obtain the particle size distributions.

The FTIR spectra were recorded in transmission mode at a resolution of 2.0 cm^{-1} on a Perkin-Elmer 2000 spectrometer (equipped with a MCT detector) with the samples in self-supporting pellets introduced in an AABSPEC 2000 cell allowing us to run the spectra *in situ* in a controlled atmosphere and temperature (from room temperature up to 600 °C).

As for the experiments at low temperature, the pelletised samples were introduced in a cell allowing thermal treatments in a controlled atmosphere and spectrum scanning at controlled temperature (from −180 °C up to room temperature). In order to mimic the activation before the catalytic tests and to follow the effect of such activation on the nature of the exposed active sites and of the species formed during methanol oxidation reaction, the catalysts were subjected to an oxidative treatment before the measurements. The thermal treatment included heating from room temperature (r.t.) up to 200 °C under outgassing below 10^{-3} mbar; an inlet of 20 mbar of oxygen and heating up to 400 °C; at 400 °C the oxygen was changed three times (20 mbar for 10 min each run). After that, the sample was cooled down to r.t. in oxygen and finally outgassed at the same temperature. For each spectrum, the spectrum of the sample before the inlet of the probe/reactants (CO, methanol or oxygen) or of the methanol/oxygen mixture was used as the background. All reported spectra were background subtracted and normalized to the density of the pellets.

EXAFS experiments were carried out on the BM23 beamline at the ESRF facility (Grenoble, France).[31] Fluorescence XAS spectra at the Au L_3-edge (11.919 keV) were collected with a 13-element Ge detector. The beam energy was selected using a double-crystal Si(111) monochromator, and the third harmonic rejection was performed using a Rh coated mirror with an angle of −2.2 mrad.[21] EXAFS signals were extracted and analyzed using the IFEFFIT package.[32] The samples were hosted inside a plug flow reactor using a 1 mm quartz capillary available on BM23 for *in situ*/*operando* measurements.[33] The experiments can be divided into two stages. Stage 1: the samples have been heated from room temperature up to 200 °C in a small furnace, then they have been treated with a mixture of O_2/He (20% O_2–He, 30 cm^3 min^{-1}) up to 400 °C. After oxygen treatment, a CO–O_2 1 : 1/He mixture (5% CO, 5% O_2) was fluxed at r.t. Stage 2: the samples were heated at 200 °C and treated with a mixture of O_2/He (20% O_2–He, 30 cm^3 min^{-1}) up to 400 °C. Successively the sample was cooled down to r.t. and a vapour of methanol/O_2/He mixture (20% O_2–He) was fluxed and finally the catalysts were heated up to 100 °C in the reaction mixture.

Results and discussion

Catalytic activity in the CH_3OH oxidation

The temperature dependence of CH_3OH conversion degree is presented in Fig. 1. The catalytic measurements indicated that the amount of promoter has a strong influence on the activity of ceria-based gold catalysts, particularly in defining the onset temperature of the catalytic activity. In particular, the activity towards the CH_3OH oxidation follows the trend: AuCe10Co > AuCe5Co > AuCe15Co > AuCe ≫ Au/Co_3O_4 ≫ Ce10Co. The light-off curve related to bare ceria doped with 10 wt% Co_3O_4 appeared at the highest temperature, giving evidence for the key role displayed by gold.

The best performance was observed in the case of the catalyst doped with 10 wt% Co_3O_4, over which almost 100% CH_3OH conversion degree at a temperature as low as 40 °C was obtained.

The comparison with the data recently reported by Scirè *et al.* (about 95% methanol conversion at 125 °C over a gold supported on ceria catalyst prepared by deposition–precipitation)[34] puts in evidence the promising application of $AuCeO_2$ catalysts doped with Co_3O_4. Moreover, a high defectivity of ceria exposed faces, along with the presence of gold nanoparticles with the smallest size and the highest hydrogen consumption during TPR experiments (*e.g.* highest oxygen mobility), was found over this AuCe10Co sample, according to our previous high resolution TEM characterization.[19]

The light-off curves for CH_3OH oxidation of Au/CeO_2 catalysts doped with Co_3O_4 were shifted to lower temperatures with respect to that of undoped Au/CeO_2 and to much lower temperatures if compared to Au/Co_3O_4, which is also the worst catalyst. This behaviour is better pointed out from the data in Table 1, where the T_{50} conversion values (*i.e.* the temperature at which 50% conversion was reached) are compared. From the data reported in Table 1, the promoting effect of Co_3O_4 is evident, together with the fact that the beneficial addition of

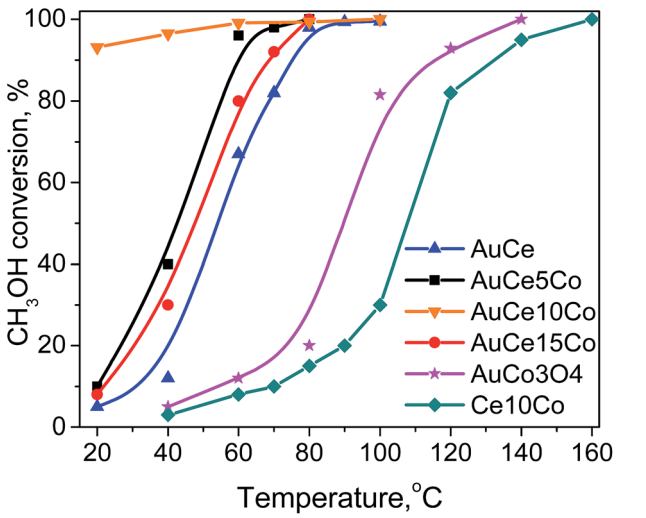

Fig. 1 Temperature dependence of CH_3OH conversion over gold catalysts on ceria doped with 5, 10 and 15 wt% Co_3O_4, over unpromoted Au/CeO_2, Au/Co_3O_4 and bare ceria doped with 10 wt% Co_3O_4.

Table 1 Extrapolated T_{50} values for CH_3OH oxidation and calculated TOFs (s^{-1}) at two different temperatures over the catalysts

Catalyst	CH_3OH oxidation (°C)	TOF at 20 °C (s^{-1})	TOF at 40 °C (s^{-1})
$AuCeO_2$	53	0.00446	0.0167
AuCe5Co	41	0.00633	0.0253
AuCe10Co	<20	0.0484	0.0505
AuCe15Co	47	0.00458	0.0172

cobalt oxide increases at low promoter content, reaches a maximum and then declines, in agreement with the fact that gold supported on the pure promoter phase (Au/Co_3O_4 sample) is the least active catalyst. In addition, it was found that the kinetic regime is not controlled by diffusional limitations. This statement is based on the experiments performed with two different catalyst pellets, the former by using a pellet with a given weight and the latter with a pellet with a double weight with respect to that employed in the first test. The methanol molar flow was also doubled and a constant weight hourly space velocity was maintained at a constant partial pressure. The same methanol conversion to CO_2 in the steady state regime indicated the absence of diffusion limitations. Table 1 also shows the turnover frequencies (TOFs), expressed as s^{-1} at two different temperatures. The TOF values were calculated according to previous considerations.[35]

Gold dispersions were calculated for all samples based on the average particle size determined by HRTEM/HAADF and reported in ref. 19 (AuCe5Co – 2.4 nm, AuCe10Co – 1.8 nm, AuCe15Co – 2.1 nm), assuming the presence of cuboctahedral particles. According to the catalytic trend for the CH_3OH conversion (see also Fig. 1), the TOF values obtained for the AuCe10Co catalyst are one order of magnitude higher than those related to the other samples. The temperature has a pronounced effect on the conversion: indeed, with the exception of AuCe10Co, the obtained TOF values increase about four times when the temperature is raised from 20 °C up to 40 °C. A very recent study on Au supported on bare ceria reported the TOF values at two different temperatures.[36] The TOF markedly increased from 3.72×10^{-5} s^{-1} at 45 °C to 1.02×10^{-4} s^{-1} at 70 °C, putting in evidence an enhancement even more accentuated, but in agreement with the data reported in Table 1. Moreover, the behaviour of AuCe5Co and AuCe15Co is very similar to the unpromoted AuCe catalyst. In contrast, in the case of AuCe10Co, the TOF value is almost unchanged, further showing that 10 wt% Co_3O_4 provides the optimal composition for the catalysis and that for this catalyst the composition plays the major role, even with respect to the temperature.

Effect of the support composition on the gold dispersion

The catalytic activity measurements revealed an almost 100% CH_3OH conversion degree at 40 °C for the AuCe10Co catalyst. Therefore, the addition of 10 wt% Co_3O_4 has improved the activity. It was previously found that the most active catalyst was that containing a large amount of Au nanoparticles with an average size of 1.8 nm.[19] Since the deposition–precipitation of gold was carried out on the already doped support, an evaluation of the influence of the presence of Co_3O_4 on the metal dispersion and size distribution was done by performing new HRTEM measurements on the most promising AuCe10Co catalyst. The results were compared with those obtained for undoped $AuCeO_2$ in order to put in evidence peculiar features arising from the different compositions of the support on which the same amount of gold has been deposited. All these data are summarized in Fig. 2. Both catalysts are supported on cubic CeO_2, mainly exposing the (111) face (not shown).

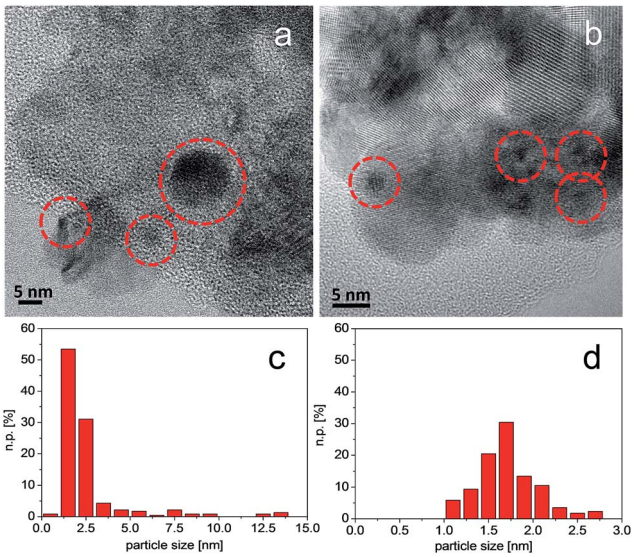

Fig. 2 HRTEM images collected on $AuCeO_2$ (section a) and AuCe10Co (section b), where the presence of Au nanoparticles is put in evidence by red circles. Au particle size distributions of $AuCeO_2$ and AuCe10Co are reported in sections c and d, where n.p. = number of particles. Instrumental magnification: 300 000× and 500 000×, respectively.

The AuCe catalyst contains gold species with heterogeneous size in the 2–12 nm range (section a, evidenced by red circles), resulting in an average diameter equal to 7.5 ± 4.5 nm (section c). However, the particle size distribution reveals that the large majority of the roundish gold nanoparticles has size around 2 nm (more than 50%).

In contrast, the AuCe10Co catalyst exposes gold nanoparticles with a smaller size (section b, evidenced by red circles), as indicated by the narrow particle size distribution, the average size being equal to 1.69 ± 0.41 nm (section d). It can be inferred that the presence of 10 wt% Co_3O_4 in the ceria support significantly affected the metal dispersion, exerting a beneficial effect on the stabilization of the Au nanoparticles during the final calcination at 400 °C and therefore favoring the formation of particles with more uniform size than in the case of $AuCeO_2$. These findings are in agreement with the enhancement in the catalytic activity observed for the catalyst doped with 10 wt% Co_3O_4.

Nature of the exposed sites and *in situ* spectra of methanol oxidation reaction

FTIR spectroscopy measurements were carried out on the bare AuCe and on AuCe10Co, *i.e.* on the most active doped sample.

This vibrational study is aimed at investigating the effect of the promoting species on the nature and the abundance of gold exposed sites and to have information on the nature of the surface species formed during methanol oxidation from r.t. up to 100 °C.

In Fig. 3a, the FTIR spectra collected upon CO adsorption at r.t. on unpromoted AuCe oxidised at 400 °C are shown.

Besides a shoulder at 2112 cm^{-1}, related to CO on partially oxidized metallic gold,[37] a broad absorption at 2138 cm^{-1} is observed after the inlet of 15 mbar CO at r.t. on AuCe (blue line). Upon CO pressure decreases at the same temperature (black lines) the band at 2138 cm^{-1} decreases in intensity without changing the position, whilst the shoulder at a lower wavenumber totally disappears. The residual absorption is irreversible to the outgassing at r.t. (down to 1.0×10^{-3} mbar, red line), giving anomalous evidence of a strong bond between CO and the involved adsorption sites, since CO is usually reversibly adsorbed on metallic gold. Some of us reported on a similar band some years ago and assigned it to CO on positively charged Au_n^+ clusters, where $4 \leq n \leq 6$ stabilized on the oxidized surface of ceria.[38] This assignment was supported by DFT calculations of Wu *et al.*,[39] showing that the adsorption energy of CO on small cationic, neutral, and anionic clusters progressively increases with the electron depletion from the cluster. Also the calculated C–O stretching frequencies supported this assignment as they increased with increasing the positive charge on the clusters. In addition, also the paper by Fanlike *et al.*,[40] in which the CO vibrational frequencies of $Au_n(CO)_m^+$ complexes in the gas phase ($3 \leq n \leq 10$ and $3 \leq m \leq 8$) have been measured experimentally, corroborated our assignment together with further spectroscopic findings. Cationic gold clusters are still present after methanol oxidation reaction, as signalled by the broad band at 2121 cm^{-1}, whilst no bands related to oxidised gold species exposed at the surface of the nanoparticles have been detected (Fig. 3b). The inlet of the CO probe at r.t. on the AuCe10Co catalyst (Fig. 3c) produced a band at 2149 cm^{-1} (red line) that despite the decrease of the CO pressure firstly increases in intensity and red shifts at 2140 cm^{-1} (orange line) and then decreases in intensity and moves to 2135 cm^{-1} (black lines down to violet line). Also in this case the residual absorption is irreversible to the outgassing at r.t. (violet line). These results indicate the absence of partially oxidized metallic gold (band at 2112 cm^{-1}),[30] showing that only cationic gold clusters with the same nuclearity as those detected on AuCe are exposed at the surface of the oxidised AuCe10Co sample before the reaction. Moreover, if the spectra are compared with those reported in section a, the amount of these species is higher on the Co-containing sample. The increased intensity of this absorption despite the reduction of the CO pressure is an indication that the small cationic gold clusters are initially covered by adsorbed oxygen and probably are in a higher oxidized state. Indeed, the inlet of the probe at r.t. produced some CO_2 by reaction of CO and oxygen adsorbed on gold clusters and big amounts of mono-, bi- and polydentate carbonate species are observed (see Fig. S1†). In contrast, only oxidised gold species exposed at the surface of the nanoparticles are observed after methanol oxidation reaction, as indicated by the presence of a band centred at 2113 cm^{-1} (Fig. 3d). It is worth noting that no CO is adsorbed at r.t. on the Ce10Co sample, indicating that neither cerium nor cobalt cations are able to adsorb the probe under our experimental conditions. However, previous experiments carried out at low temperature demonstrated the presence of Ce^{4+} at the surface of both samples. Interestingly, the presence of bands related to Co^{x+} cations was hardly hypothesized on AuCe10Co.[19]

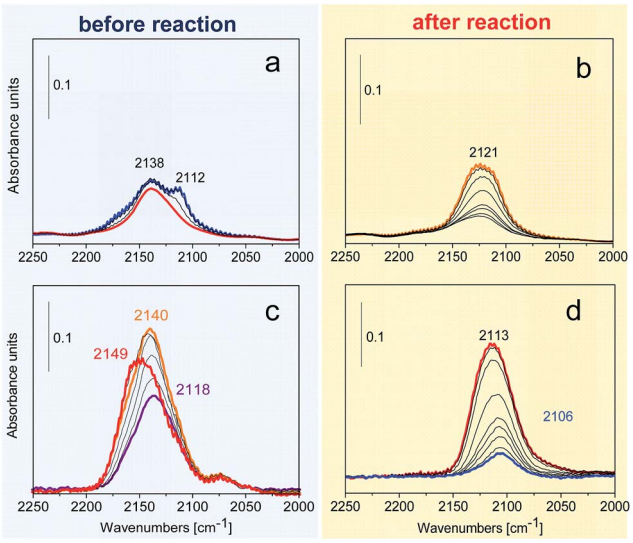

Fig. 3 FTIR difference spectra collected upon CO inlet (15 mbar) at r.t. and subsequent pressure decreases down to 1.0×10^{-3} mbar on AuCe and on AuCe10Co before (sections a and c) and after (sections b and d) methanol oxidation reaction. The spectra are normalised to the density of the pellets.

The AuCe and AuCe10Co catalysts were brought into contact with methanol (5 mbar) and then oxygen (5 mbar) at r.t. and then the temperature was gradually increased up to 100 °C in order to follow the formation (and the possible evolution) of surface species during methanol oxidation by *in situ* FTIR spectroscopy. Notwithstanding that *in situ* conditions, under static equilibrium pressure of the reactants, are far away from the ideal *operando* conditions where reactants are sent in a plug-flow reactor, FTIR spectroscopy can provide insights into both spectators and intermediate species formed on the different catalysts. Firstly, the inlet of methanol at r.t. on AuCe and AuCe10Co (blue lines in Fig. S2†) produced different amounts of on top, doubly (two species) and triply bridged methoxy species, as summarised in Table 2, where the vibrations related to the methoxy species adsorbed on AuCe and on AuCe10Co catalysts are reported. The evolution of the methoxy species at increasing temperature is shown in Fig. S2† (from brown to red lines). On top and different doubly bridged methoxy species have been detected in both samples,[41,42] starting from room temperature (blue line) up to 50 °C (brown lines), then a marked increase in the intensity of the bands related to on top methoxy species is observed at 75 °C (violet lines). Methoxy species are definitely more abundant on AuCe10Co than on AuCe, in particular the intensity of the absorptions due to the doubly bridged methoxy species with different coordinations of Ce

Table 2 Wavenumbers for vibrations of on top, doubly (two species) and triply bridged methoxy species adsorbed on AuCe and on AuCe10Co catalysts

Vibrational modes	$\nu_a(CH_3)$ cm^{-1}	$2\delta(CH_3)$ cm^{-1}	$\nu_s(CH_3)$ cm^{-1}	$\nu(OC)$ cm^{-1}
On top methoxy species				
AuCe	2911	2884	2801	1105
AuCe10Co	2911	2881	2800	1105
Doubly bridged methoxy species				
AuCe	2923	2834	2800	1050
AuCe10Co	2936	2838	2801	1053
Doubly bridged methoxy species with different coordinations of Ce cations with oxygen ions				
AuCe	2910	2841	2807	1039
AuCe10Co	2911	2838	2809	1038
Triply bridged methoxy species				
AuCe	2934	2847	—	1026
AuCe10Co	2949	2836	—	1023

cations with oxygen ions (bands at 1053 and 1038 cm^{-1}) seems enhanced on AuCe10Co, further indicating that the addition of cobalt leads to a lower degree of coordination of the ceria surface sites of the doped sample and as a consequence to an enhanced reactivity towards the same amount of methanol. It has been reported that methoxy species formed upon methanol dissociation over CeO_2 behave both as spectators and intermediate species, depending on their proximity to gold nanoparticles.[36] It can be proposed that on AuCe10Co, that is the most active catalyst, the higher is the metal dispersion, the larger is the amount of active methoxy species acting as reaction intermediates.

The above findings are also in agreement with the results of the previous analysis of the HRTEM diffraction fringes related to the ceria-containing phases, indicating an increase of about four times of the spacings due to defective ceria phases for AuCe10Co (37.35%) if compared to AuCe (10.77%).[19]

The presence of more defective ceria may also favour the formation of double bridged reactive methoxy species on the surface of the catalyst. In addition, triply bridged methoxy species are easily distinguishable on AuCe10Co also at 100 °C,[25,26] whilst they are almost depleted at the same temperature on AuCe, as indicated by the weak bands at 1026, 2847 and 2934 cm^{-1}. These features further indicate that, due to the presence of cobalt, AuCe10Co displays a more easy activation of methanol and an enhanced reactivity of methoxy species if compared to AuCe.

The FTIR spectra collected on AuCe and on AuCe10Co in contact with the methanol/oxygen mixture at increasing temperature are reported in Fig. 4 sections a and b, respectively.

On the AuCe sample, the methanol oxidation was mainly limited to the production of bidentate (bands at 2845, 1572, 1549, 1398, 1371 cm^{-1}) and monodentate (bands at 1605 and 1250 cm^{-1}) formate species.[43] However, bands related to monodentate (1507 and 1358 cm^{-1}), bidentate (1564, 1299, 1022, 856 cm^{-1}) and polydentate (1475, 1053 and 833 cm^{-1}) carbonate species[27] start to increase in intensity at 75 °C, simultaneously with the decrease of the bands related to methoxy species (see Fig. 5 and S2,† where the methoxy region in the 1150–950 cm^{-1} region is zoomed).

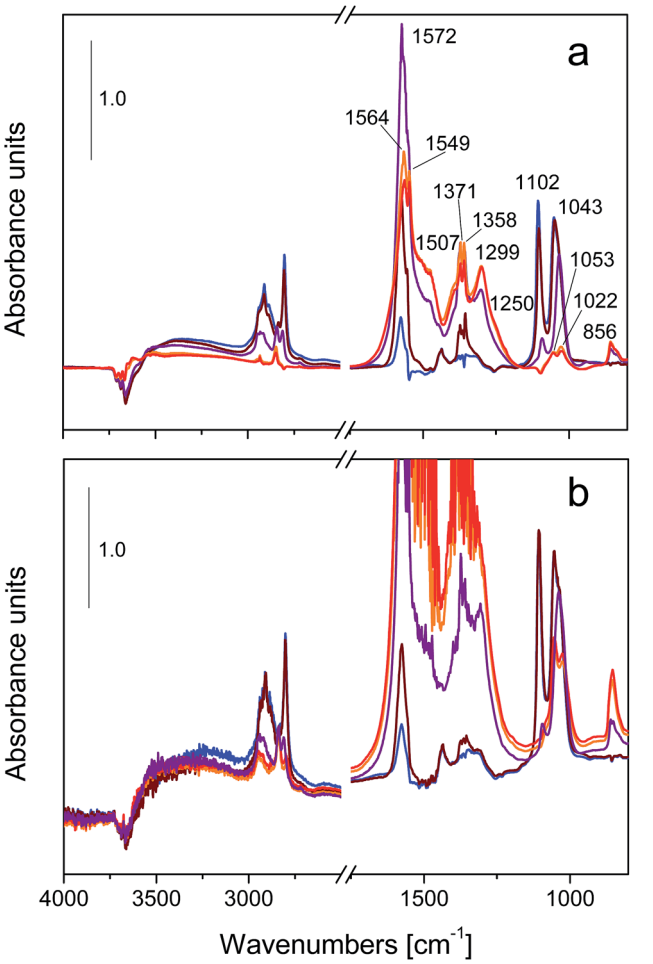

Fig. 4 FTIR difference spectra collected on AuCe (section a) and AuCe10Co (section b) in contact with the methanol/oxygen mixture after 10 min at r.t. (blue lines), at 50 °C (brown lines), 75 °C (violet lines), at 100 °C (orange lines) and after 20 min (red lines) at the same temperature.

The FTIR results put in evidence that on both catalysts methanol reacted with the surface giving rise to different methoxy species at r.t. and to formates at 50 °C. These species further evolved into mono-, bi- and polydentate carbonates by increasing the temperature at 75 °C and up to 100 °C. On AuCe10Co larger amounts of carbonates are produced.

Differently from what was previously observed in a combined steady state isotopic transient kinetic analysis and *operando* FTIR study,[36] bands related to the presence of carbonate species were also detected due to the adopted experimental conditions (static conditions rather than flow conditions reported in the literature[36]). The presence of carbonates indicates that formate species are converted into CO_2 that evolves into surface carbonates under static conditions, whereas they would be flushed away in dynamic flow. The comparison between *in situ*

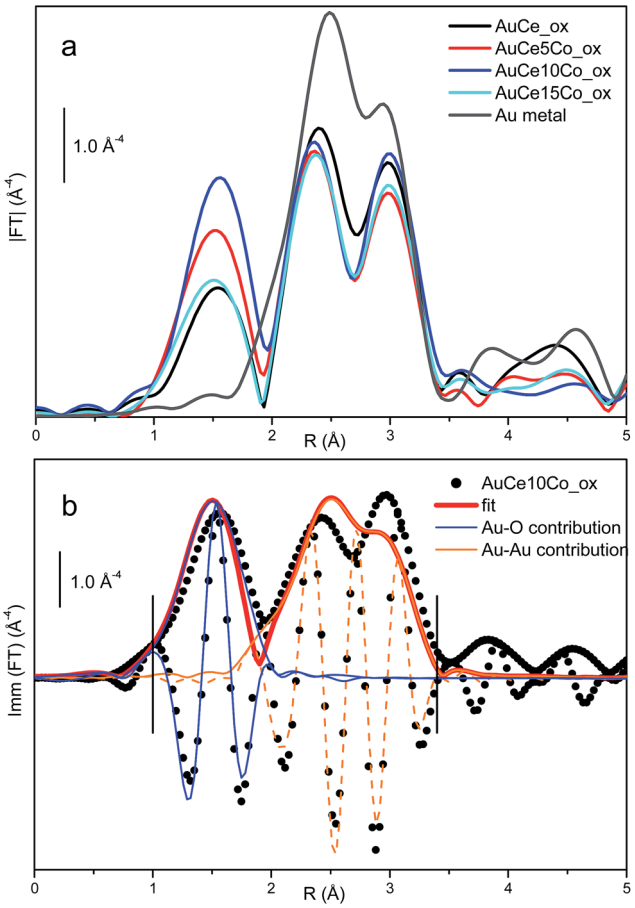

Fig. 5 Section (a): modulus of k^3-weighted, phase uncorrected, FT of the Au L_3-edge EXAFS spectra of the catalysts prepared on differently Co doped ceria substrates and submitted to thermal treatment in oxygen at 400 °C. Corresponding imaginary parts are reported in Fig. S5.† Section (b): comparison between the experimental (scattered black dots) and the best fit (red full line) for AuCe10Co_ox. Also reported are the imaginary parts of the experimental data (scattered black dots) and the modulus (full lines) and the imaginary parts (dashed lines) of the individual Au–O (blue lines) and Au–Au (orange lines) contributions.

and *operando*[36] experiments indicates that both methoxy and formate species are intermediates and not simply spectators.

The thermal methanol decomposition was also performed on both catalysts in order to compare the results with experiments carried out without oxygen: it was observed that on AuCe on top methoxy species disappeared along with the formation of formate species at 100 °C, simultaneously to the conversion of doubly bridged methoxy with different coordinations into more coordinated doubly bridged methoxy species (Fig. S3†). Therefore, the methoxy species with different coordinative unsaturation could be related to the formate production. In contrast, in the case of AuCe10Co no formate species have been observed and only very intense bands due to carbonate-like species are produced (Fig. S4†), whereas the behaviour of the methoxy species is the same as observed on AuCe for the same reaction. These results demonstrate that in the absence of oxygen as a reactant, the AuCe10Co catalyst is able to efficiently provide oxygen to decompose methanol, further confirming that on this system the addition of Co causes significant enhancement in the reducibility, which resulted in improved oxidation activity.[18] However, the same reaction carried out on the bare Ce10Co support did not give rise to any product (Fig. S5†) indicating that there must be a positive synergy involving gold to enhance oxygen mobility and activation.

It has been reported that promoting supported gold nanoparticles with lanthanum oxide largely increases the hydrogen selectivity in the partial oxidation of methanol, due to the fact that La_2O_3 was found to facilitate the reduction of initially present oxidic gold species.[44] If compared with the results related to AuCe, the CO adsorption experiments at room temperature revealed the presence of more positivized gold sites on AuCe10Co before methanol oxidation reaction (Fig. 3c). These sites could be responsible for the enhanced reactivity displayed by AuCe10Co and also appear to be reduced to a higher extent after reaction (Fig. 3d), demonstrating that an effect of the addition of cobalt on gold is occurring.

Insights into the structure of the active sites

In order to investigate the effect of Co addition to the ceria substrate on the average local environment of supported gold (5, 10 and 15 wt%), Au L_3 edge EXAFS experiments were performed on the AuCe, AuCe5Co, AuCe10Co and AuCe15Co catalysts previously submitted to a thermal treatment in O_2 at 400 °C, that is, the activation procedure which the catalyst underwent before the catalytic tests.

The k^3-weighted, phase uncorrected, FT of the EXAFS spectra collected on all catalysts are shown in Fig. 5, section a. The analogous spectrum collected on Au foil is also reported for comparison (grey line).

All spectra are characterized by two main contributions. The first one, appearing in the 1.0–2.0 Å region and having a maximum at about 1.55 Å, is due to the single scattering Au–O of an Au oxide phase. The second one that appears in the 2.0–3.5 Å region and, independently of the presence of two maxima at 2.39 and 2.98 Å, is mainly due to the first shell single scattering Au–Au of supported metal nanoparticles.[45] This assignment is supported by the imaginary parts of the FT (see Fig. S6†). Moreover, the AuCe10Co catalyst shows the highest intensity of the Au–O component due to the interaction between the active gold nanoparticles and the oxygen atoms of the oxidic support. This EXAFS evidence is in accordance with the FTIR characterization results discussed here and with previous high angle annular dark field observations that revealed the smallest average size of gold particles on this catalyst if compared to AuCe5Co and AuCe15Co.[19,46]

The quantitative results obtained from the EXAFS fits on all the samples are summarized in Table 3.

The quantitative results confirm what was observed previously on the simple basis of the intensity of the Au–O component at 1.55 Å: the sample with the highest oxidized fraction is AuCe10Co, followed by AuCe5Co and then by AuCe15Co, which is comparable with the undoped AuCe. Conversely, no trend can be put in evidence for the Au–Au contributions that are formally

Table 3 Results of the fit performed on oxidized samples[a]

	CN		σ^2 (Å^2)		R (Å)			
	Au–O	Au–Au	Au–O	Au–Au	Au–O	Au–Au	E_0 (eV)	R factor
AuCe	1.2 ± 0.3	5.5 ± 1.1	0.006 ± 0.001	0.004 ± 0.002	1.96 ± 0.02	2.854 ± 0.012	5.3 ± 2.2	0.002
AuCe5Co	1.7 ± 0.3	4.6 ± 0.5			1.95 ± 0.01	2.848 ± 0.006		0.006
AuCe10Co	2.2 ± 0.4	5.0 ± 0.6			1.94 ± 0.02	2.852 ± 0.008		0.010
AuCe15Co	1.2 ± 0.2	4.7 ± 0.3			1.95 ± 0.01	2.850 ± 0.004		0.003

[a] $S_0^2 = 0.85$ fixed from the value extracted from the fit of the Au foil ($S_0^2 = 0.85 \pm 0.8$); Δk = (3.3–10.0) Å^{-1} and ΔR = (1.4–3.5) Å, resulting in a number of independent points larger than 11.

equivalent within the experimental error bars. It should be noted that in this case the intensity of the Au–Au contribution is inversely proportional to the fraction of the oxidized phase discussed above but is also influenced by the different particle size distributions,[47,48] so that the two effects cannot be directly disentangled in a straightforward manner. On top of these the region between 2.0 and 3.5 Å is expected to host also the higher shell contributions from the oxide phase that have been neglected in these refinements. This fact also explains the minor discrepancy between the experimental data and fit reported in Fig. 5b.

The methanol oxidation reaction was then investigated on the Au10CoCe sample, being the most active catalyst: the first set of spectra was collected at room temperature. Furthermore, starting from the catalysts previously oxidized, another set of spectra was recorded under *operando* conditions, flowing methanol and oxygen, starting from room up to 120 °C. Au/CeO_2 was measured as the reference sample, too. Three subsequent $\chi(k)$ spectra were measured at each temperature, to evaluate the experimental uncertainty.[49] The data analysis was performed on the averaged $\chi(k)$ spectrum by non-linear fitting procedures. Fig. 6 shows the k^3 weighted, phase uncorrected FT (module and imaginary part) of the AuCe10Co sample collected during methanol oxidation reaction at 120 °C (black scattered points). The signal due to the Au–O distance at 1.55 Å disappears during the reaction,[50] while a new contribution at about 1.8 Å is observed. The component at large distances (2.0–3.5 Å range) is clearly due to Au–Au contributions, whereas the new component around 1.8 Å is associated with an Au–Co contribution. The EXAFS fit of the experimental data performed assuming such a structural model (red line in Fig. 6) clearly shows the good agreement with the experimental spectrum, validating the presence of Co in the first coordination shell of a fraction of Au atoms. The quantitative results of the fit are reported in Table 4. The EXAFS study, corroborated by FTIR measurements, performed on all catalysts indicates that oxidized gold species are involved in the methanol reaction (Fig. 5 and related data analysis in Table 3). In addition, the EXAFS analysis of the catalyst under the working conditions (Fig. 6) suggests that the active sites present on the most active sample (with 10 wt% Co_3O_4) are those where gold sites are strongly interacting with Co. On these active sites reactive oxygen species, possibly close to Co sites, can be activated and participate in the oxidative dehydrogenation reaction of methanol to formate species.[36] Moreover, due to the synergistic effect between cobalt and gold, the AuCe10Co catalyst is also able to provide reactive oxygen species under the reaction conditions: reduced gold species close to oxygen vacancies and in strong interaction with cobalt ions are formed after the reaction. Such Au species are those located at the interface with the support. These features can be at the origin of the enhanced catalytic activity of AuCe10Co.

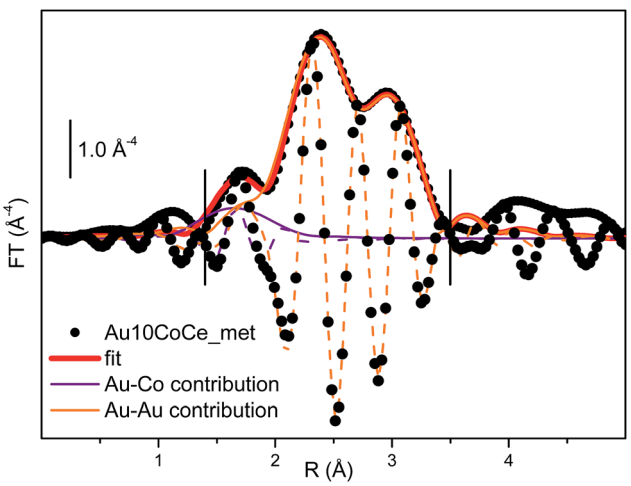

Fig. 6 Modulus of the k^3-weighted, phase uncorrected, FT of the Au L_3-edge EXAFS spectrum of AuCe10Co collected during methanol oxidation reaction at 120 °C (black scattered dots) compared with the fit (red curve). Also reported are the imaginary parts of the experimental data (black scattered dots) and the modulus (full lines) and the imaginary parts (dashed lines) of the individual Au–Co (purple lines) and Au–Au (orange lines) contributions.

Table 4 Result of the fit performed on the AuCe10Co_met EXAFS spectrum[a]

Paths	CN	σ^2 (Å^2)	R (Å)	E_0 (eV)
Au–Co	0.3 ± 0.1	0.010 ± 0.001	2.09 ± 0.03	3.6 ± 0.7
Au–Au	8.8 ± 0.8		2.835 ± 0.007	

[a] $S_0^2 = 0.85$ fixed from the value extracted from the fit of the Au foil ($S_0^2 = 0.85 \pm 0.8$); Δk = (3.3–10.0) Å^{-1} and ΔR = (1.4–3.5) Å, resulting in a number of independent points larger than 11; R factor = 0.005.

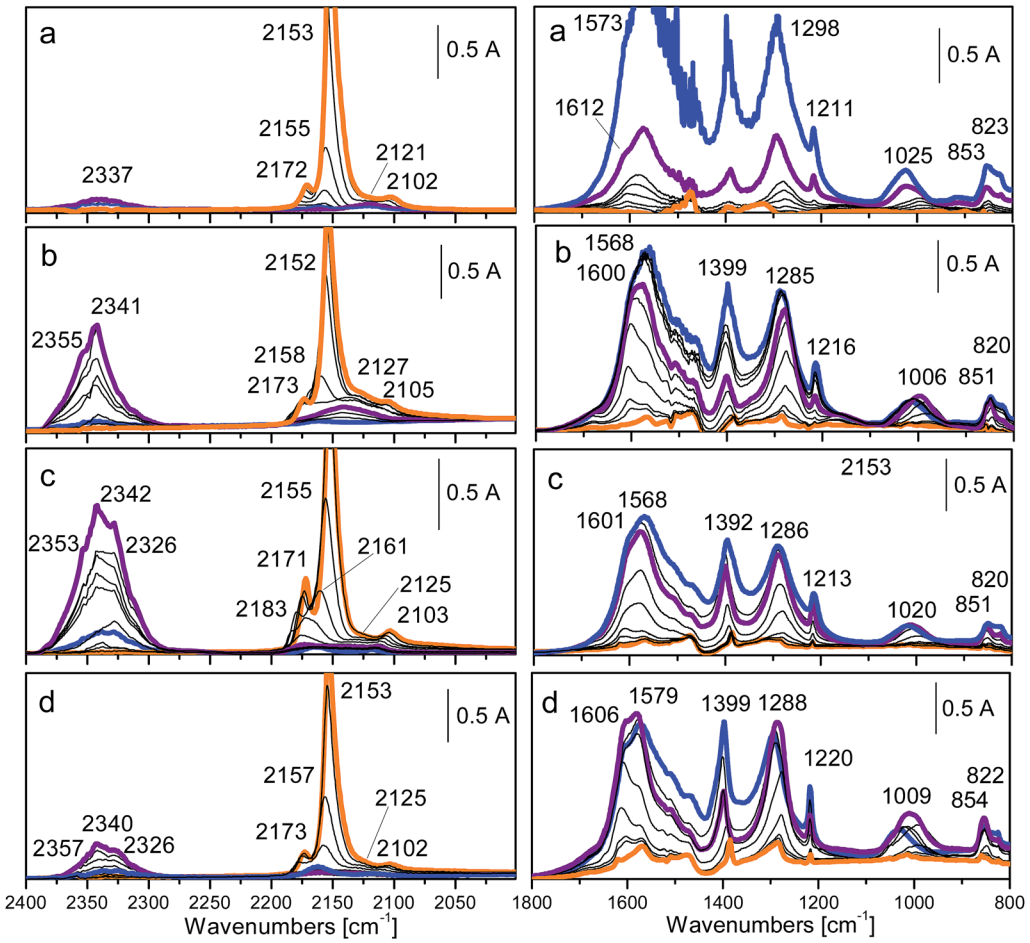

Fig. 7 Evolution of FTIR difference spectra collected on AuCe (section a), AuCe5Co (section b), AuCe10Co (section c) and AuCe15Co (section d) oxidised at 400 °C immediately after the inlet of $^{18}O_2$ at −180 °C on preadsorbed CO (orange lines) and at increasing contact times and temperature (black and purple lines) up to room temperature (blue lines) in the 2000–2400 cm^{-1} (left) and in the 1800–800 cm^{-1} (right) regions. The spectrum collected before CO dosage has been used to obtain the reported difference spectra, which have been normalised to the density of the pellets.

Promotional role of Co in oxygen mobility

Spectroscopic evidence for the effect of the support composition on the oxygen mobility is reported in Fig. 7, where the evolution of the bands during CO and $^{18}O_2$ interaction on all the samples is shown starting from −180 °C (orange lines, *i.e.* immediately after the inlet of $^{18}O_2$ on preadsorbed CO), during the heating (black and purple lines) and up to room temperature (blue lines).

The inlet of $^{18}O_2$ at increasing diffusion times and temperature (black and purple lines up to blue line) over the samples previously saturated by CO at −180 °C (orange line) caused an erosion from the low-frequency side of the band at about 2102–2105 cm^{-1}, due to CO on Au particles covered by adsorbed oxygen,[37] a gradual decrease in intensity of the component at 2121–2127 cm^{-1} due to CO adsorbed on cationic gold clusters[38–40] and the rapid depletion of the bands related to the support (component at 2150 cm^{-1} due to CO in interaction with OH groups and bands at 2155–2161 cm^{-1} and at 2171–2173 cm^{-1} due to CO on different Ce^{4+} sites[43]). Only in the case of AuCe10Co a band at 2183 cm^{-1}, tentatively assigned to CO adsorbed on Co^{x+} sites,[51] is observed during the heating at room temperature. Simultaneously, bands related to CO_2 formation during CO oxidation are produced at higher frequencies (asymmetric CO_2 stretching or ν_3 mode[52]). Such absorptions have the highest intensity in the case of AuCe10Co (section c) and their intensity follows the same trend as for the catalytic activity: AuCe10Co > AuCe5Co > AuCe15Co > AuCe. In greater detail, the three isotopomers of the CO_2 molecule were observed: a growing band at 2326 cm^{-1}, assigned to the $C^{16}O^{18}O$ solid-like phase, accompanied by bands at 2340–2342 and at 2353–2357 cm^{-1}, assigned to $C^{16}O_2$ and $C^{18}O_2$ solid-like phase, respectively.[53] The spectra showed that a rapid exchange between the oxygen of ceria and the $^{18}O_2$ molecules coming from the gas phase occurred already at low temperature. Moreover, the high intensity of the band ascribed to $C^{16}O_2$ indicated that oxygen participating in the reaction at low temperature mainly comes from the support, putting in evidence the fact that the catalyst promotion with Co led to increased oxygen mobility because of the improved exchange properties of the ceria support.

The results demonstrated the enhanced ability of the Co-promoted-ceria support to supply active lattice oxygen that is

beneficial for the reaction and were in good agreement with already published TPR results[17] for the highest hydrogen consumption and shift of T_{max} to lower temperature observed in the profile of the AuCe10Co sample. Here we recall that these experiments were performed on catalysts oxidised at 400 °C, *i.e.* the temperature used for the activation before performing the catalytic tests on CH_3OH oxidation, see Fig. 1, Table 1 and related discussion.

On the stability of the catalysts

The analysis of the spectra reported in Fig. 7 (right) indicated that on all the samples mainly two kinds of carbonate-like species were formed simultaneously with the production of CO_2 (see the spectra reported in the right parts of Fig. 7). Such species have different abundances, depending on the composition of the four catalysts. Hydrogen carbonates with peaks at 1600–1612 cm^{-1}, 1392–1399 cm^{-1} and the component around 1020 cm^{-1} (νCO_3 modes), at 820–823 cm^{-1} (πCO_3) and at 1211–1220 cm^{-1} (δOH) were detected.[43] In addition, bidentate carbonates are also produced, as revealed by the absorptions at 1568–1579 cm^{-1}, at 1285–1298 cm^{-1} and at 1006–1009 cm^{-1} (νCO_3 modes) and at 851–854 cm^{-1} (πCO_3).[43] Please note that approximately in the 1350–1400 cm^{-1} region there must be the symmetric CO_2 stretching (or ν_1 mode) of the CO_2 molecules giving rise to the ν_3 mode (complex band at 2320–2360 cm^{-1} discussed above). For symmetry reason this band is IR inactive for CO_2 molecules in the gas phase, but becomes IR active upon surface adsorption because of symmetry break. However, as the absorption coefficient of the ν_1 mode of adsorbed CO_2 is typically one order of magnitude lower than that of the ν_3 mode,[52] we can neglect their presence in the spectra reported in the right parts of Fig. 7.

Summarizing this isotopically labelled IR study, it is found that the presence of another oxide besides ceria has a remarkable influence on the intensity of the bands in the carbonate region: on the AuCe catalyst (section a) the highest amount of hydrogen carbonate as well as of bidentate carbonate species is adsorbed on the surface after the reaction if compared to the Co-promoted catalysts. Indeed, the intensity of such bands decreases with increasing the amount of produced CO_2, giving evidence that cobalt oxide lowers the basicity of ceria and therefore the carbonate species formation is inhibited, despite the CO_2 formation. AuCe10Co is the most active catalyst, but also the most stable one, due to the highest amount of produced CO_2 and the lowest amount of carbonate-like species present at the surface after the reaction. This represents a remarkable achievement for the promotion of the gold on ceria catalyst with Co, as in most of the cases in catalysis an increase of the catalyst activity is accompanied by a faster deactivation time and compromises must be found between these two aspects of promotion.

Conclusions

The catalytic performance in methanol oxidation of different gold catalysts supported on ceria modified by the addition of Co_3O_4 was investigated. Au/CeO_2 and Au/Co_3O_4 were also studied as reference samples. A strong influence of the amount of the Co promoter was observed. The activity trend followed the order: AuCe10Co > AuCe5Co > AuCe15Co > AuCe $\gg$ Au/Co_3O_4. TOFs have been calculated for all catalysts, and it was found that the TOF values obtained for AuCe10Co are one order of magnitude higher than those related to the other catalysts. Moreover, with the exception of AuCe10Co, for which the TOF value is almost unchanged, the conversion is strongly dependent on the temperature.

Different *in situ* FTIR experiments were performed. Adsorption of CO on AuCe and AuCe10Co indicate that oxidized gold sites are initially present on both activated samples, suggesting that such species are involved in the methanol reaction. Upon CH_3OH dosage, different methoxy groups are formed on both catalysts at r.t. (more abundantly on AuCe10Co). After successive O_2 addition they are consumed on both catalysts starting at about 75 °C and giving rise to mainly formate species on AuCe and to large amounts of different carbonate species on AuCe10Co. Moreover, the synergy between gold and Co-promoted ceria support causes significant enhancement of reducibility and capability for oxygen activation, which resulted in improved oxidation activity, as demonstrated by the FTIR experiments carried out in the absence of oxygen. The capability of AuCe10Co to supply active oxygen species involves the participation of the oxygen vacancies on modified ceria as well as of the surface of a separate, highly reducible, CoO_x phase.

As suggested by EXAFS analyses, the active sites present on the best performing AuCe10Co catalyst are oxidized gold species at the interface with the support and close to Co sites, which are able to activate and to react with oxygen giving rise to the formation of formate species and of carbonate species. The presence of a multiplet of bands in the CO_2 asymmetric stretching region after CO interaction with $^{18}O_2$ clearly reveals that the promotion of ceria by Co facilitates the exchange reaction with the $^{16}O_2$ atoms of the support. Moreover, it is demonstrated that the production of carbonate species is lowered in the presence of cobalt oxide, despite the increase in CO_2 formation. Such results give evidence for the improved stability of the Co-promoted catalysts.

The correlation of the catalytic activity and of a well-defined metal dispersion with the findings, provided by *in situ* FTIR and *operando* EXAFS studies about the nature and structure of the active sites, allows us to bridge the gap of experimental data previously obtained by HAADF, XRD, FTIR, TPR and to clarify the precise nature of the synergy between the gold phase and the Co-promoted ceria support, which resulted in excellent CH_3OH oxidation activity.

Acknowledgements

M. Manzoli and F. Vindigni gratefully acknowledge the IIT (Istituto Italiano di Tecnologia) for financial support (NANO GOLD Project). The Bulgarian authors gratefully acknowledge the financial support by the Bulgarian National Science Fund (Project DFNI T 02/4). C. Lamberti acknowledges the Megagrant of the Russian Federation Government to support scientific research at the Southern Federal University, no. 14.Y26.31.0001.

References

1 S. Scire and L. F. Liotta, *Appl. Catal., B*, 2012, **125**, 222–246.
2 T. Tabakova, G. Avgouropoulos, J. Papavasiliou, M. Manzoli, F. Boccuzzi, K. Tenchev, F. Vindigni and T. Ioannides, *Appl. Catal., B*, 2011, **101**, 256–265.
3 A. Taketoshi and M. Haruta, *Chem. Lett.*, 2014, **43**, 380–387.
4 M. Melchionna and P. Fornasiero, *Mater. Today*, 2014, **17**, 349–357.
5 P. Dutta, S. Pal, M. S. Seehra, Y. Shi, E. M. Eyring and R. D. Ernst, *Chem. Mater.*, 2006, **18**, 5144–5146.
6 T. Tabakova, L. Ilieva, I. Ivanov, R. Zanella, J. W. Sobczak, W. Lisowski, Z. Kaszkur and D. Andreeva, *Appl. Catal., B*, 2013, **136**, 70–80.
7 O. H. Laguna, A. Perez, M. A. Centeno and J. A. Odriozola, *Appl. Catal., B*, 2015, **176**, 385–395.
8 F. Vindigni, M. Manzoli, T. Tabakova, V. Idakiev, F. Boccuzzi and A. Chiorino, *Appl. Catal., B*, 2012, **125**, 507–515.
9 C. Pojanavaraphan, A. Luengnaruemitchai and E. Gulari, *Int. J. Hydrogen Energy*, 2013, **38**, 1348–1362.
10 O. H. Laguna, M. A. Centeno, G. Arzamendi, L. M. Gandia, F. Romero-Sarria and J. A. Odriozola, *Catal. Today*, 2010, **157**, 155–159.
11 L. Ilieva, T. Tabakova, G. Pantaleo, I. Ivanov, R. Zanella, D. Paneva, N. Velinov, J. W. Sobczak, W. Lisowski, G. Avdeev and A. M. Venezia, *Appl. Catal., A*, 2013, **467**, 76–90.
12 T. R. Reina, S. Ivanova, V. Idakiev, J. J. Delgado, I. Ivanov, T. Tabakova, M. A. Centeno and J. A. Odriozola, *Catal. Sci. Technol.*, 2013, **3**, 779–787.
13 T. R. Reina, A. A. Moreno, S. Ivanova, J. A. Odriozola and M. A. Centeno, *ChemCatChem*, 2012, **4**, 512–520.
14 A. Alvarez, S. Ivanova, M. A. Centeno and J. A. Odriozola, *Appl. Catal., A*, 2012, **431**, 9–17.
15 X. W. Xie, Y. Li, Z. Q. Liu, M. Haruta and W. J. Shen, *Nature*, 2009, **458**, 746–749.
16 Y. Liu, B. C. Liu, Q. Wang, C. Y. Li, W. T. Hu, Y. X. Liu, P. Jing, W. Z. Zhao and J. Zhang, *J. Catal.*, 2012, **296**, 65–76.
17 B. C. Liu, Y. Liu, C. Y. Li, W. T. Hu, P. Jing, Q. Wang and J. Zhang, *Appl. Catal., B*, 2012, **127**, 47–58.
18 L. Ilieva, P. Petrova, T. Tabakova, R. Zanella, M. V. Abrashev, J. W. Sobczak, W. Lisowski, Z. Kaszkur and D. Andreeva, *Catal. Today*, 2012, **187**, 30–38.
19 T. Tabakova, D. Dimitrov, M. Manzoli, F. Vindigni, P. Petrova, L. Ilieva, R. Zanella and K. Ivanov, *Catal. Commun.*, 2013, **35**, 51–58.
20 H. J. Freund, *Angew. Chem., Int. Ed.*, 1997, **36**, 452–475.
21 S. Bordiga, E. Groppo, G. Agostini, J. A. van Bokhoven and C. Lamberti, *Chem. Rev.*, 2013, **113**, 1736–1850.
22 C. Garino, E. Borfecchia, R. Gobetto, J. A. van Bokhoven and C. Lamberti, *Coord. Chem. Rev.*, 2014, **277**, 130–186.
23 J. A. van Bokhoven and C. Lamberti, in *X-Ray Absorption and X-Ray Emission Spectroscopy: Theory and Applications*, ed. J. A. van Bokhoven and C. Lamberti, John Wiley & Sons Ltd, Hoboken, NJ, 2016, vol. 2, ch. 13, pp. 353–383.
24 A. I. Frenkel, *Chem. Soc. Rev.*, 2012, **41**, 8163–8178.
25 A. I. Frenkel, C. W. Hills and R. G. Nuzzo, *J. Phys. Chem. B*, 2001, **105**, 12689–12703.
26 C. Lamberti, E. Groppo, G. Spoto, S. Bordiga and A. Zecchina, *Adv. Catal.*, 2007, **51**, 1–74.
27 A. Vimont, F. Thibault-Starzyk and M. Daturi, *Chem. Soc. Rev.*, 2010, **39**, 4928–4950.
28 C. Lamberti, A. Zecchina, E. Groppo and S. Bordiga, *Chem. Soc. Rev.*, 2010, **39**, 4951–5001.
29 S. Bordiga, C. Lamberti, F. Bonino, A. Travert and F. Thibault-Starzyk, *Chem. Soc. Rev.*, 2015, **44**, 7262–7341.
30 M. Manzoli and F. Vindigni, in *Gold Catalysis*, ed. L. Prati and A. Villa, Pan Stanford Publishing Pte. Ltd., Singapore, 2016, ch. 8, pp. 205–252.
31 O. Mathon, A. Beteva, J. Borrel, D. Bugnazet, S. Gatla, R. Hino, I. Kantor, T. Mairs, M. Munoz, S. Pasternak, F. Perrin and S. Pascarelli, *J. Synchrotron Radiat.*, 2015, **22**, 1548–1554.
32 M. Newville, *J. Synchrotron Radiat.*, 2001, **8**, 96–100.
33 S. J. A. Figueroa, D. Gibson, T. Mairs, S. Pasternak, M. A. Newton, M. Di Michiel, J. Andrieux, K. C. Christoforidis, A. Iglesias-Juez, M. Fernandez-Garcia and C. Prestipino, *J. Appl. Crystallogr.*, 2013, **46**, 1523–1527.
34 S. Scirè, P. M. Riccobene and C. Crisafulli, *Appl. Catal., B*, 2010, **101**, 109–117.
35 S. Ivanova, V. Pitchon, C. Petit and V. Caps, *ChemCatChem*, 2010, **2**, 556–563.
36 I. Castellanos, P. Bazin, S. Thomas, O. Marie and M. Daturi, *Top. Catal.*, 2016, **59**, 337–346.
37 F. Boccuzzi, A. Chiorino, M. Manzoli, P. Lu, T. Akita, S. Ichikawa and M. Haruta, *J. Catal.*, 2001, **202**, 256–267.
38 M. Manzoli, F. Boccuzzi, A. Chiorino, F. Vindigni, W. Deng and M. Flytzani-Stephanopoulos, *J. Catal.*, 2007, **245**, 308–315.
39 X. Wu, L. Senapati, S. K. Nayak, A. Selloni and M. Hajaligol, *J. Chem. Phys.*, 2002, **117**, 4010–4015.
40 A. Fielicke, G. von Helden, G. Meijer, D. B. Pedersen, B. Simard and D. M. Rayner, *J. Am. Chem. Soc.*, 2005, **127**, 8416–8423.
41 A. Badri, C. Binet and J. C. Lavalley, *J. Chem. Soc., Faraday Trans.*, 1997, **93**, 2121–2124.
42 C. Binet and M. Daturi, *Catal. Today*, 2001, **70**, 155–167.
43 C. Binet, M. Daturi and J. C. Lavalley, *Catal. Today*, 1999, **50**, 207–225.
44 B. P. C. Hereijgers, T. M. Eggenhuisen, K. P. de Jong, H. Talsma, A. M. J. van der Eerden, A. M. Beale and B. M. Weckhuysen, *J. Phys. Chem. C*, 2011, **115**, 15545–15554.
45 J. T. Miller, A. J. Kropf, Y. Zha, J. R. Regalbuto, L. Delannoy, C. Louis, E. Bus and J. A. van Bokhoven, *J. Catal.*, 2006, **240**, 222–234.
46 N. Weiher, E. Bus, L. Delannoy, C. Louis, D. E. Ramaker, J. T. Miller and J. A. van Bokhoven, *J. Catal.*, 2006, **240**, 100–107.
47 G. Agostini, A. Piovano, L. Bertinetti, R. Pellegrini, G. Leofanti, E. Groppo and C. Lamberti, *J. Phys. Chem. C*, 2014, **118**, 4085–4094.
48 G. Agostini, R. Pellegrini, G. Leofanti, L. Bertinetti, S. Bertarione, E. Groppo, A. Zecchina and C. Lamberti, *J. Phys. Chem. C*, 2009, **113**, 10485–10492.

49 C. Lamberti, S. Bordiga, D. Arduino, A. Zecchina, F. Geobaldo, G. Spano, F. Genoni, G. Petrini, A. Carati, F. Villain and G. Vlaic, *J. Phys. Chem. B*, 1998, **102**, 6382–6390.
50 W. Deng, A. I. Frenkel, R. Si and M. Flytzani-Stephanopoulos, *J. Phys. Chem. C*, 2008, **112**, 12834–12840.
51 K. I. Hadjiivanov and G. N. Vayssilov, *Adv. Catal.*, 2002, **47**, 307–511.
52 E. Garrone, B. Bonelli, C. Lamberti, B. Civalleri, M. Rocchia, P. Roy and C. O. Arean, *J. Chem. Phys.*, 2002, **117**, 10274–10282.
53 T. Tabakova, M. Manzoli, F. Vindigni, V. Idakiev and F. Boccuzzi, *J. Phys. Chem. A*, 2010, **114**, 3909–3915.